
Article:
Koc, M., Sun, T. orcid.org/0000-0002-5518-0315 and Wang, J. (2016) Performance Improvement of Direct Torque Controlled IPM Drives by Employing a Linear Combination of Current and Voltage Based Flux Observers. IET Power Electronics. ISSN 1755-4535

https://doi.org/10.1049/iet-pel.2015.0891

Performance Improvement of Direct Torque Controlled IPM Drives by Employing a Linear Combination of Current and Voltage Based Flux Observers

Mikail Koc[1*], Tianfu Sun[1], Jiabin Wang[1]

[1]Electrical Machines and Drives Group, The University of Sheffield, Sheffield, United Kingdom
[*]mikaelkoc@gmail.com

Abstract: Flux observers in direct torque controlled (DTC) motor drives are of paramount importance as the drives rely on estimated variables for feedback control. It is well known that current based (CB) estimations are advantageous at low speeds, whereas voltage based (VB) estimations are more accurate at high speeds. Hence, a large number of state-of-the-art DTC drives utilize closed loop flux observers in which the CB and VB estimations become dominant at low and high speeds, respectively. However, it has been discovered that the performance and current waveforms with the closed loop observers significantly deteriorate at low speeds since the residual error of the VB estimation causes current distortions. In addition, these observers have nonlinear flux transition trajectory resulting in reduced accuracy during transitions. To improve the low speed performance and achieve the linear transition, an alternative combination of the two estimations is proposed. Experimental results on a 10kW interior mounted permanent magnet (IPM) machine drive designed for electric vehicle traction applications validate significant improvements on the drive performance.

1.Introduction

Electric vehicles are likely to become an important alternative for personal mobility in near future as they facilitate the use of renewable energy technologies [1]. The IPM motors are increasingly used [2, 3] in various applications including traction applications due to their superior characteristics such as high efficiency, low noise, low rotor losses, robustness due to buried magnets, high field weakening (FW) capability, and high torque density.

However, IPM machines exhibit highly non-linear characteristics due to magnetic saturations, and the machine parameters such as inductances and permanent magnet flux linkage are current and temperature dependent. The operation and temperature dependent characteristics pose a great challenge for control of IPM drives to achieve fast dynamic response and energy efficient operation [4].

Control of IPM machines can be classified into 2 categories: field oriented control (FOC) and direct torque control (DTC). Whilst the FOC drives are usually realized in the rotor (dq) reference frame [5], DTC drives may be realized in a synchronous or stationary reference frame depending on how the controlled variables, torque and flux, are observed. A typical DTC implementation is formulated in the stator flux reference frame ($f\tau$) which rotates at the synchronous speed. The relationship between the dq and $f\tau$ reference frames is shown in Fig. 1, where the angular displacement between the d axis and f axis is denoted by δ. Both frames rotate in synchronism with the rotor angle, θ_e, and the stator flux angle, $\theta_f = \theta_e + \delta$, respectively.

FOC drives rely on measured currents, whereas DTC drives are dependent on observer quality for feedback control. Thus, the observer dynamic response and accuracy is of paramount importance in DTC drives [6]. It is well known in the literature that the CB estimations are advantageous at low speeds and the VB estimation perform better at high speeds. In those drives which employ only the VB estimations [7, 8], the machine operation is investigated either above certain speeds or the estimation is manually switched from CB to VB modes of operation. Hence, for a wide speed range of operation, closed loop flux observers which combine current and voltage based estimations have been developed in [9] and employed extensively in recent work on IPM [10-21], surface mounted permanent magnet [16, 22], synchronous reluctance [16] and induction machine [9, 16, 23] drives.

Whilst the aim of the closed loop observers is to take advantages of CB and VB estimations at low and high speeds, respectively, it has been discovered through detailed studies by the authors that the interference between the two modes exists in these observers. This may result in significant degradation of drive performance at low speeds where the inverter nonlinearity and voltage drop across stator resistance become dominant. Accordingly, although the CB estimation is expected to be dominant, the residual error of the extremely poor VB estimation may cause significant distortions on the current waveforms leading to a poor torque control quality.

A second issue of the conventional observers is that the estimated flux follow a nonlinear transition trajectory from CB to VB mode and vice-versa. This results in poor performance during transitions since the observer accuracy reduces due to the momentous nonlinearity. Despite the linearization of the trajectory has been studied in [23], none of the above drives have employed the linearization technique due to the implementation complexity. Hence, a large number of recent drives still suffer from the nonlinear transitions.

To overcome the issues associated with deteriorated drive performance at low speeds and nonlinear transition trajectory between the two modes, an alternative combination is proposed in this paper. In the proposed approach, CB and VB modes of estimations are not combined in a closed loop manner, on the contrary, two estimators are combined in such a way that the transition from one to other follows a linear trajectory. By doing so, the two major problems; cross-interferences and poor transitions are avoided together with a much simpler combination. It is noteworthy that despite the closed loop observers sound to perform better, in fact, the drive system itself is closed loop in either cases whether the observer is closed or open loop.

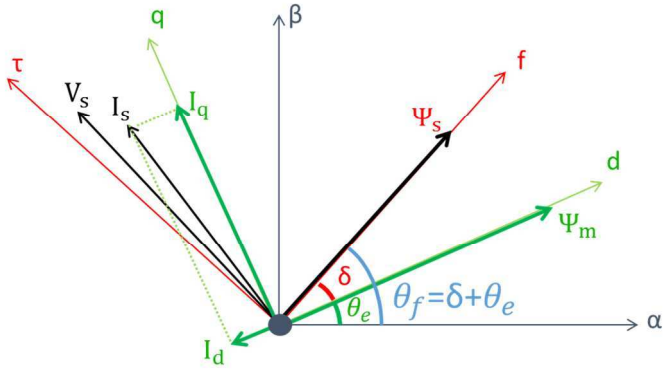

Fig. 1 *Stationary (αβ), rotor (dq) and stator flux (fτ) reference frames*

2.Mathematical Model of IPM Machines in Stator Flux Frame

Transformation from the rotor frame to the stator flux frame can be obtained from Fig. 1 as follows:

$$\begin{bmatrix} F_f \\ F_\tau \end{bmatrix} = \begin{bmatrix} cos\delta & sin\delta \\ -sin\delta & cos\delta \end{bmatrix} \begin{bmatrix} F_d \\ F_q \end{bmatrix} \quad (1)$$

where $\boldsymbol{F}$ can be any current, voltage or flux linkage vector. δ is known as the torque angle as it is proportional to torque and it is constant in steady-states. Hence, the well-known dq-axis mathematical modelling can be transformed to the $f\tau$ frame by (1) so that the following equations are obtained [13]:

$$V_f = RI_f + \frac{d\Psi_s}{dt} \tag{2}$$

$$V_\tau = RI_\tau + w_e\Psi_s + \frac{d\delta}{dt}\Psi_s \tag{3}$$

$$T_e = \frac{3p}{2}\Psi_s I_\tau \tag{4}$$

where (V_f, V_τ) and (I_f, I_τ) denote the voltage and current vectors in the $f\tau$ frame, respectively. Ψ_s is the magnitude of stator flux vector, R is the phase resistance, p is the number of pole-pairs, w_e is the electrical angular speed, T_e is the electromagnetic torque.

3.Stator Flux Oriented Control System Configuration

1.1. Controlled State Variables

It is clearly seen from (2) and (3) that the stator flux magnitude and the torque angle can be controlled by V_f and V_τ voltage vectors, respectively. It has been extensively shown that torque can be controlled directly [24] in stator flux frame oriented drives. Hence, electromagnetic torque and stator flux magnitude errors are regulated in the system to generate reference voltages.

Fig. 2 illustrates the schematic of the direct torque controlled IPM machine drive where '*' and '^' denote reference and estimated values, respectively. The stator flux magnitude for MTPA operation is generated by a predefined LUT whose input is demand torque. The reference and estimated state variables are illustrated in 'red' and 'blue' colours, respectively.

1.1. Current and Voltage Constraints

Unlike classical FOC drives, current limitation cannot be imposed directly in DTC drives since currents are not the controlled variables. Instead, torque limit may be imposed for indirect limitation of the currents. Equations (5) and (6) give voltage and current constraints, respectively, in the $f\tau$ reference frame.

$$|V| = \sqrt{V_f^2 + V_\tau^2} \leq V_{max} \tag{5}$$

$$|I| = \sqrt{I_f^2 + I_\tau^2} \leq I_{max} \tag{6}$$

Rearranging (6), one can obtain the τ- axis current constraint in (7). Substituting (7) into (4) yields the limit for electromagnetic torque in (8). Further, the stator flux magnitude limit can be derived by considering steady-state and substituting (2) and (3) into (5), and it is given in (9).

$$I_\tau \leq \sqrt{{I_{max}}^2 - {I_f}^2} \tag{7}$$

$$T_e \leq \frac{3}{2} p \Psi_s \sqrt{{I_{max}}^2 - {I_f}^2} \tag{8}$$

$$\Psi_s \leq \frac{\sqrt{{V_{max}}^2 - \left(RI_f\right)^2} - RI_\tau}{w_e} \tag{9}$$

Therefore, the voltage and current limits are imposed by (5) and (8), respectively, and FW may be triggered by (9) automatically in DTC based control schemes. Over-modulation (OM) block in Fig. 2 illustrates the voltage limitation based on (5). The differences between inputs and outputs of the OM block are fed back to the PI controllers to prevent the integrators from winding-up. The coupling term ($w_e\Psi_s$) in (3) may be compensated in the feed-forward as shown in Fig. 2. The reference voltages are transformed to the stationary frame before being fed to the space vector modulation (SVPWM).

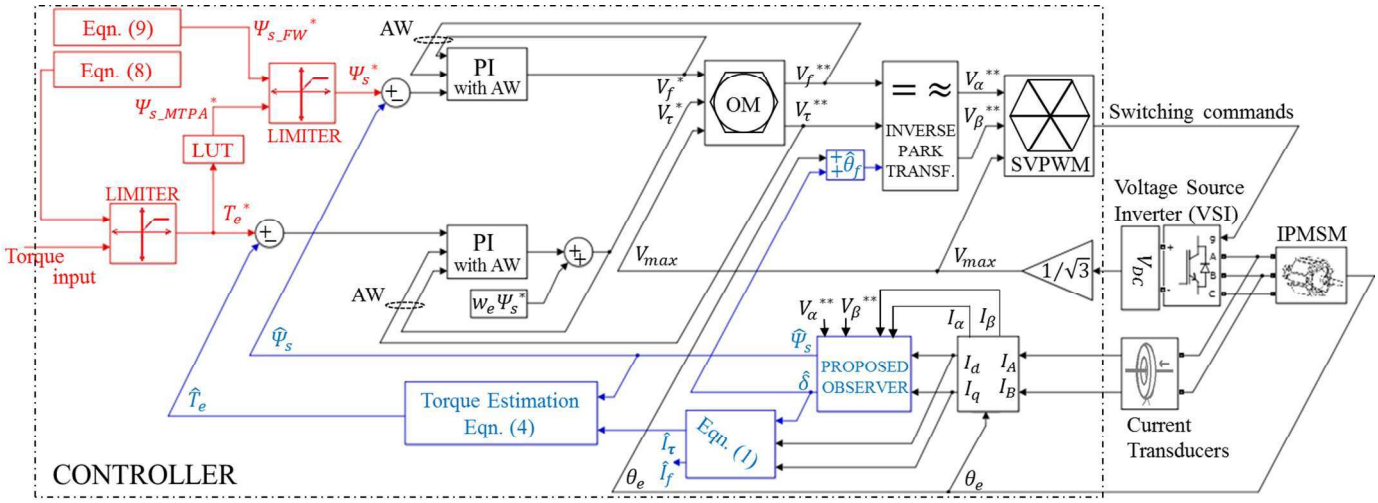

Fig. 2 *Schematic of the DTC drive*

3.3 Observers for Feedback Control

3.3.1 Current Based (CB) Flux Estimation: The well-known dq-axis flux linkage modelling are given by:

$$\begin{bmatrix}\Psi_d\\ \Psi_q\end{bmatrix}=\begin{bmatrix}L_d & 0\\ 0 & L_q\end{bmatrix}\begin{bmatrix}I_d\\ I_q\end{bmatrix}+\begin{bmatrix}\Psi_m\\ 0\end{bmatrix} \tag{10}$$

where $[\Psi_d \quad \Psi_q]^T$ denotes the dq-axis flux linkages. Ψ_m is the magnetic flux linkage, L_d and L_q are the dq-axis inductances, respectively. The stator flux vector, *i.e.* the amplitude and the phase angle (δ-Fig. 1) is obtained by substituting (10) into (1).

3.3.2 Voltage Based (VB) Flux Estimation: Integration of the induced voltage (E) gives the flux linkage. From this point of view, the stator flux linkages can be estimated based on the stationary frame voltages and the currents as follows:

$$\Psi_\alpha=\int(V_\alpha-RI_\alpha)dt \quad \& \quad \Psi_\beta=\int(V_\beta-RI_\beta)dt \tag{11}$$

In general, the inverter reference voltages are employed for estimations as shown in Fig. 2 since the measurement of the discrete phase voltages is costly due to the additional hardware requirement. Accordingly, the estimation is very poor at low speeds where the inverter nonlinearity becomes prominent. Because pure integration in (11) does not work due to drifting, the integrators are commonly replaced by low-pass filters (LPF) [25] together with phase and magnitude compensations as depicted in Fig. 3 where w_c and w_e are cut-off frequency of LPFs and electrical speed in rad/s, respectively. It should be noted that the compensation outputs should be appropriate to that of the integration output as the aim is to integrate the induced voltages. It is noteworthy that high cut-off frequency may give rise to torque and flux oscillations whilst low cut-off frequency results in slow response. Hence, there is a trade-off between response time and response quality. Cartesian to polar coordinate transformation of the estimated flux linkages give the stator flux vector, *i.e.* the amplitude and the phase angle ($\theta_f=\theta_e+\delta$ in Fig. 1).

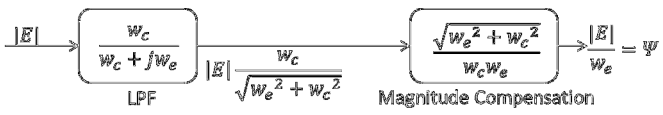

a

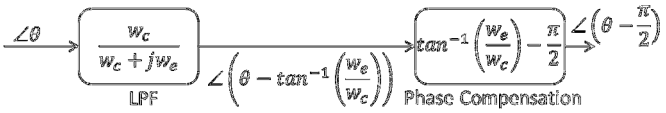

b

Fig. 3 *Magnitude and phase compensations of LPF outputs*
a Magnitude compensation
b Phase compensation

3.3.3 Conventional Closed Loop Flux Observers: The simplified block scheme of these observers, which are commonly referred to as Gopinath style closed loop observers, is given in Fig. 4-(a) [9] and the linearization of the flux trajectory to improve the observer is depicted in Fig. 5-(a) [23]. The output of both observers is given by:

$$\hat{\vec{\Psi}}_s = \big(1 - F(s)\big)\hat{\vec{\Psi}}_{s\_CB} + F(s)\hat{\vec{\Psi}}_{s\_VB} \tag{12}$$

where, $F(s)$ is the characteristic equation whose frequency response is tuned by the PI control parameters for input selection. It should be noted that "closed-loop" merely means that the combination of the two estimations is made through a feedback mechanism. Fig. 4-(b) and (c) illustrate the Bode magnitude plots of $F(jw)$ and $[1 - F(jw)]$, respectively, for conventional observer [9] with a cut-off frequency of 25Hz. Similarly, Fig. 5 (b) and (c) illustrate them for the observer with linear flux trajectory [23]. As can be seen on the magnitude (abs) plots, at low speeds when frequency is low, $F(jw) \approx 0$, and hence the CB mode is dominant. At high speeds, $[1 - F(jw)] \approx 0$ and the VB mode becomes dominant. However, it is seen on the magnitude (dB) plots that the attenuations of the two modes are finite. Consequently, the cross interferences of the two modes are only avoided at standstill and infinite speed. It is worth noting that the interference of the VB mode is much more significant than the other since the poor performance of the VB mode at low speeds may result in significant current distortions.

In addition to the cross-interference issue, it is seen in Fig. 4-(c) that the transition between the two modes is very poor and nonlinear, and hence reduces the accuracy of the observer during transitions. Although this has been addressed as shown in Fig. 5-(c), a large number of recent papers on DTC drives still suffer from the poor transitions because of the implementation complexity of linearization. This paper proposes a much simpler linear flux transition avoiding cross-interferences as well.

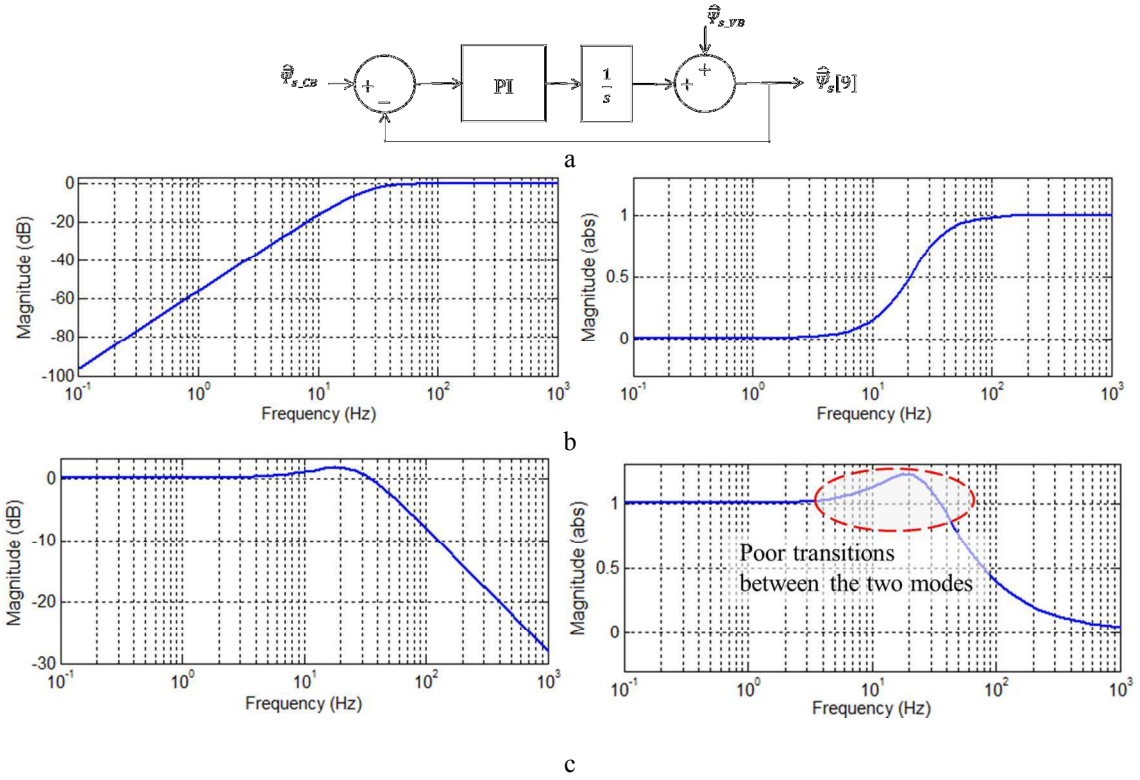

a

b

c

Fig. 4 *Schematic and Bode magnitude plots of conventional observer* [9]
a Simplified block scheme
b Bode magnitude plot of $F(jw)$
c Bode magnitude plot of $[1 - F(jw)]$

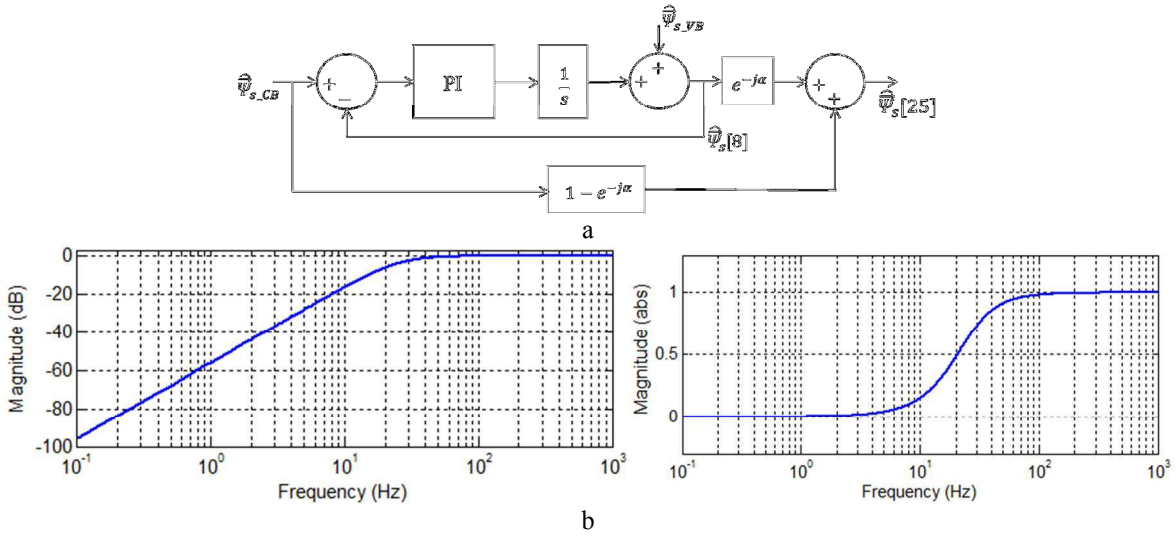

a

b

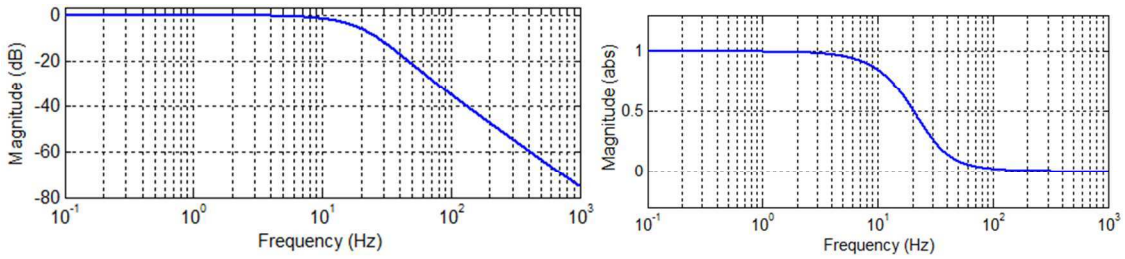

c

Fig. 5 *Schematic and Bode magnitude plots of conventional observer with linear flux trajectory* [23]
a Simplified block scheme
b Bode magnitude plot of $F(jw)$
c Bode magnitude plot of $[1 - F(jw)]$

The cross interference issue has been further investigated by simulation studies in order to validate how seriously it may deteriorate DTC drive performance employing conventional Gopinath style closed loop observers. The motor and the inverter specifications are listed in Table I and II, respectively. A high fidelity machine model [26] which accounts magnetic saturation and the effects of slotting of a real IPM machine has been employed and the inverter nonlinearities have been represented in the simulations, and hence the results are very close to a real world drive. The system shown in Fig. 2 has been implemented with the conventional observer [9] and the drive was simulated at 25 r/min speed and 40 Nm torque. It is seen from Fig. 6-a that although the estimated flux (output of the conventional observer) appears to follow the reference flux reasonably well, the actual flux, which cannot be measured in a practical drive, is heavily distorted and exhibits peak distortion 6-times in the fundamental period as shown in Fig. 6-b. This is indeed caused by the 6-step voltage distortion which results from inverter nonlinearity. Despite of the low magnitude of $F(jw) \approx 0.01$ in (12) associated with the VB mode, the extremely poor VB estimation shown in Fig. 6-(c) results in poor performance of the drive. The flux distortion gives rise to significant current waveform distortions, Fig. 6-d, that matches well with the experimental results which will be given in section 4. Because of the distorted current waveforms, the estimated flux by the CB mode is also distorted as shown in Fig. 6-(e). As will be seen, although deviation of the stator flux magnitude due to inverter nonlinearity is ~5 mWb or ~4%, the consequences are quite significant. This is because in an IPM when the magnetic saturation is relatively high, the current deviation due to the flux error will be more than 4% [10]. Since the torque is the product of flux and current, the resultant torque deviation will be more than

8%. Further, the observed flux deviation caused by the inverter nonlinearity in the VB mode introduces a large distortion in both current and torque waveforms. Therefore, inaccurate estimation of the VB mode must be completely attenuated in order to avoid the system performance deterioration.

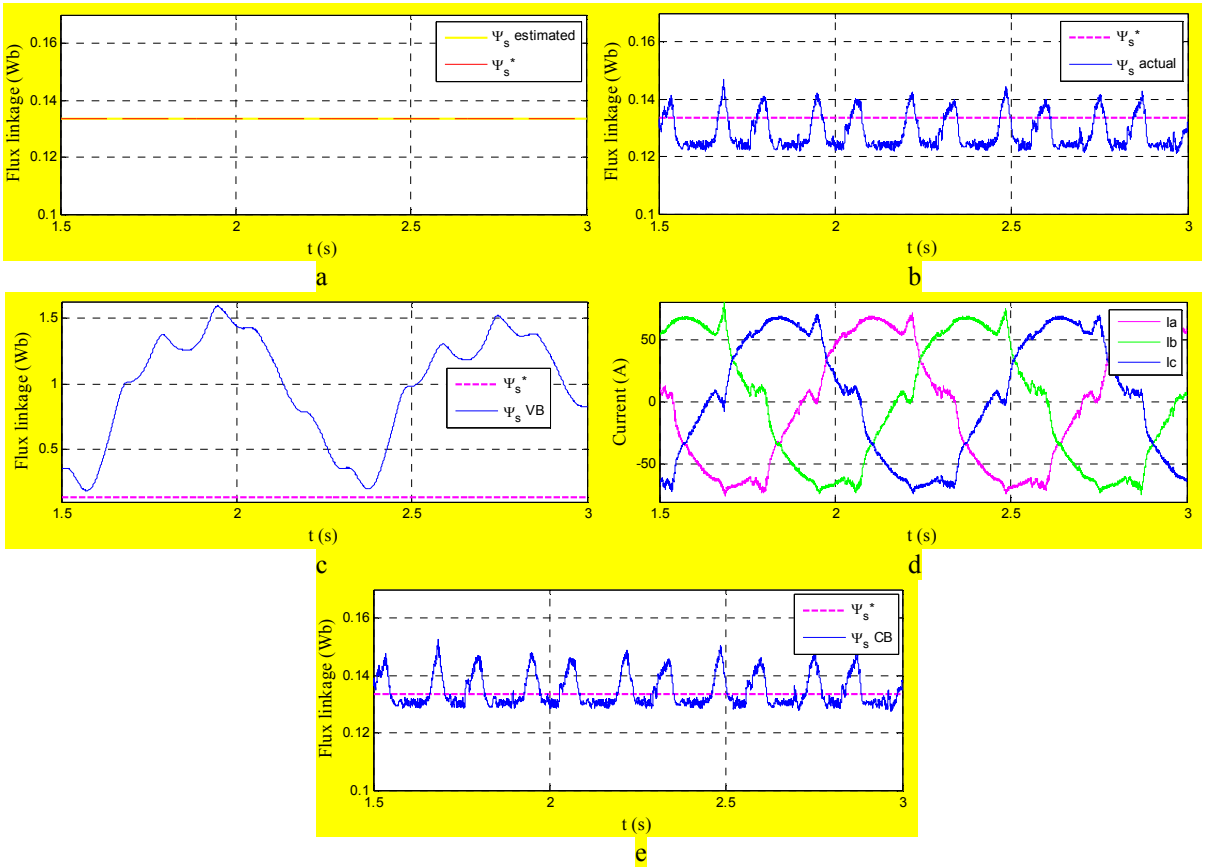

Fig. 6 *Simulation results of conventional drives at 25 r/min and 40 Nm*
a Estimated flux (observer output)
b Actual flux
c Estimated flux (VB mode)
d Current waveforms
e Estimated flux (CB mode)

Table I Prototype IPM machine specifications

Number of pole-pairs/Nominal phase resistance	3 / 0.0512 Ω
Continuous current/maximum current	58.5 A / 118 A
DC link voltage	120 V
Base speed / maximum speed	1350/4500 r/min
Continuous torque / peak torque	35.5/70 Nm
Peak power below base speed	10 kW
Peak power at maximum speed	7 kW

Table II Inverter specifications

T_s - Sampling period	125μs (8kHz)
T_d - Dead-time to prevent shoot-through	3μs
V_{Th}^S - Threshold voltage of active switch	0.85 V
V_{Th}^D - Threshold voltage of freewheeling diode	0.8 V
R_{ON}^S - On-state resistance of active switch	5 mΩ

R_{ON}^{D} - On-state resistance of freewheeling diode	4.5 mΩ

3.3.4 Proposed Approach: Because the cross-interferences of the two estimations in closed loop observers may cause significant performance deteriorations and there is poor transition performance between the two modes, an alternative combination is proposed. To circumvent the problems associated with the CB estimations, the inductances and PM flux linkage in (10) are modelled as functions of d- and q- axis currents [27] based on the experimentally calibrated FE data of the machine under study, and they are stored as look-up tables. VB estimation is processed by Fig. 3 and the current and voltage based estimated flux vectors are combined in (13) to form the output of the proposed technique.

$$\hat{\bar{\Psi}}_s = \begin{cases} \hat{\bar{\Psi}}_{s\_CB} & w \le w_{CB} \\ \hat{\bar{\Psi}}_{s\_CB}\dfrac{w_{VB}-w}{\ell} + \hat{\bar{\Psi}}_{s\_VB}\dfrac{w-w_{CB}}{\ell} & w_{CB} < w < w_{VB} \\ \hat{\bar{\Psi}}_{s\_VB} & w \ge w_{VB} \end{cases} \tag{13}$$

where w_{CB} and w_{VB} are the predefined speeds where CB and VB modes are enabled or suspended. w is the operating speed and it can be either electrical speed or mechanical speed in rad/s or in r/min as long as all speeds in (13) are in the same unit. ℓ is the length of the transition speed between w_{CB} and w_{VB} to avoid sudden change of the estimated variables. Higher the length makes the transition smoother but increases the effect of the poor performing mode. Hence, the trade-off can be optimized for a certain drive. Theoretically, the transition speed could be chosen based on the speed where the VB estimation is more accurate than the CB. Fig. 7 illustrates the transition trajectory of the flux vector $\hat{\bar{\Psi}}_s$ in the complex plane when speed increases from w_{CB} to w_{VB}. It is seen that when speed is in the midpoint (w_{mp}), the estimated output vector with the proposed approach follows the shortest path between the two vectors *i.e.* $\gamma_1 = \gamma_2$. Hence, the linear transition trajectory is achieved with a much simple combination.

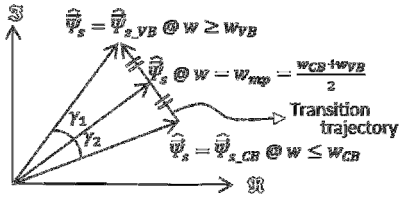

Fig. *7 Schematic of the estimated flux vector transition of the proposed approach in complex domain*

4.Experimental Results

4.1 Test Rig

In order to validate the superiority and performance improvement of the proposed drive by comparing to conventional schemes, a test rig with a 10kW IPM machine drive has been established as shown in Fig. 8. The mechanical setup, *i.e.*, the IPM machine, torque transducer and dynamometer are shown in Fig. 8-(a), and the power electronics converter setup, *i.e.*, the controller, inverter and current transducers are shown in Fig. 8-(b).

The machine whose specifications are listed in Table I is controlled in torque control mode and the speed is loaded by the dynamometer. The rotor position is measured by a magnetic encoder and the current waveforms are captured by a power analyser.

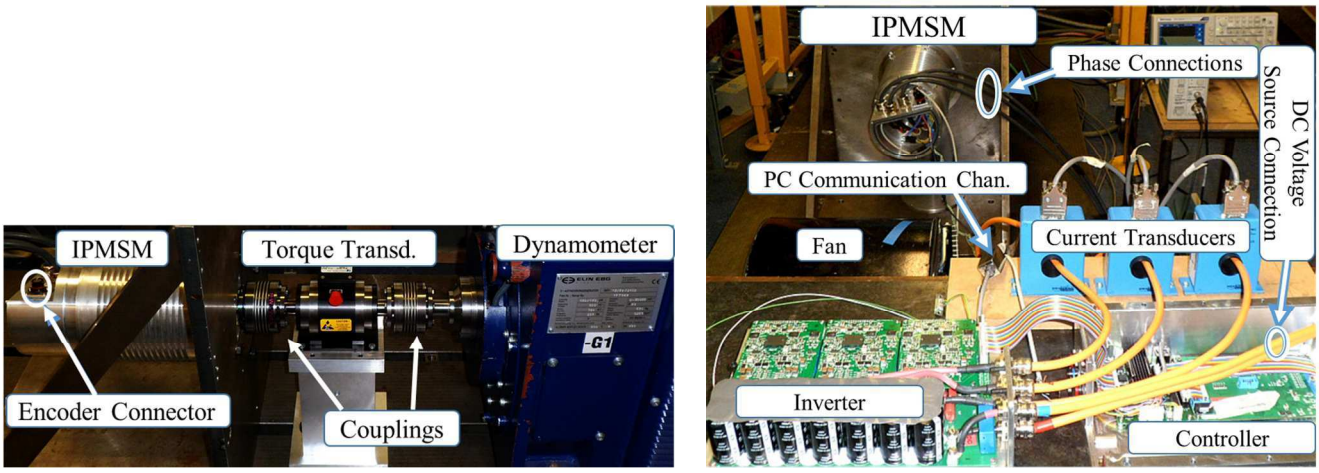

a b

Fig. ***8*** *View of the experimental hardware setup*
a Mechanical setup
b Power electronics converter setup

4.2 Low Speed Performance Comparison

In order to validate the performance improvements, the drives were performed with three observer options given in section 3.3.3 and 3.3.4 at 15 Nm torque and 25, 100, 200 r/min speeds. The results are illustrated in Fig. 9. The transition speed is adjusted to 500 r/min (=25Hz electrical frequency as shown in Fig. 4 and Fig. 5 b-c) in the drives so that the CB and VB modes are dominant below and above 500 r/min, respectively. It is seen from the experimental results that the drives with the conventional observers

are significantly vulnerable to poor performing VB estimation at low speeds. Although the PI gains of the 2 conventional observers were tuned same for 500 r/min transition speed, the drive with the linear flux trajectory is more effected by cross interference. In contrast, the issue has been avoided in the proposed approach and the current waveforms being much improved with a linear combination. Experiments at different speed and load conditions were also performed and the results are similar to those shown in Fig. 9.

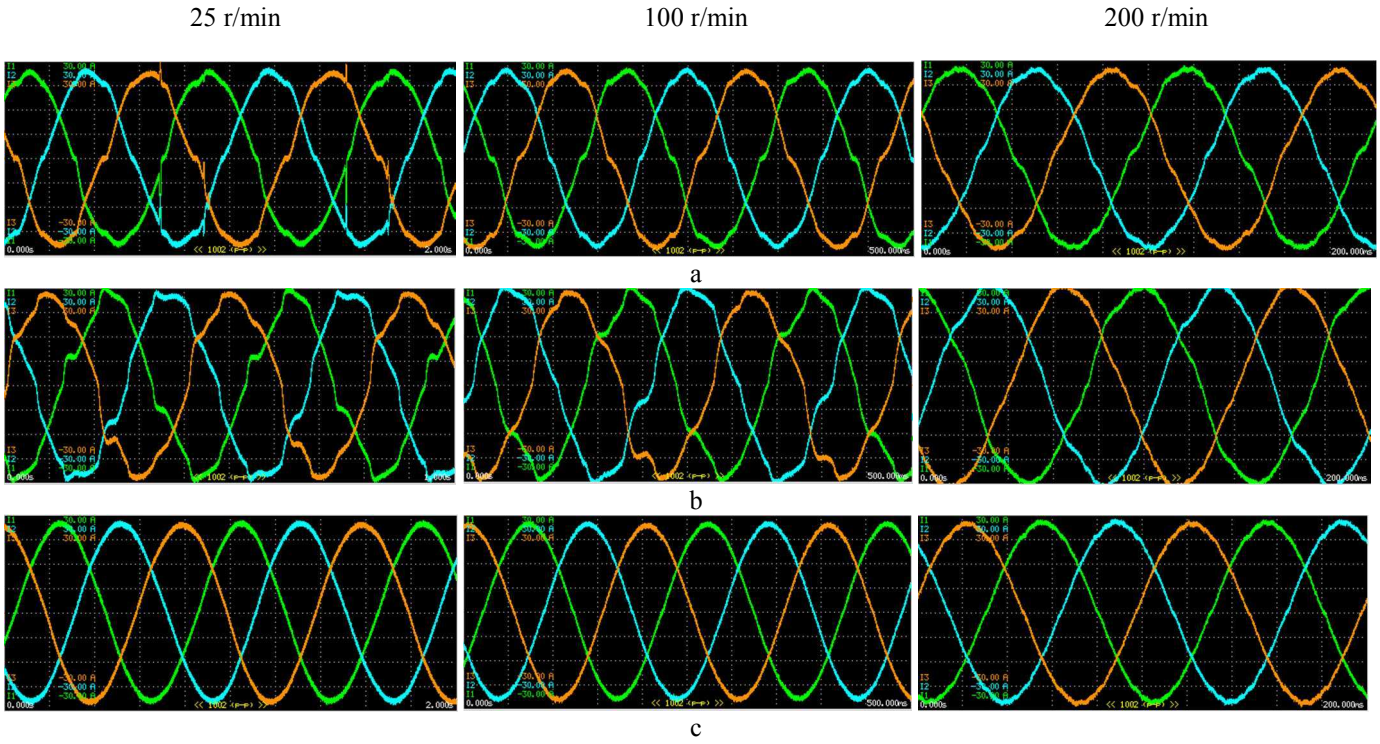

Fig. 9 *Current waveforms of drives at 15Nm torque*
a Conventional observer [9]
b Conventional observer with linear flux trajectory [23]
c Proposed combination with linear flux trajectory

4.3 Transition Performance Validation

The robustness of the drive with the proposed technique is validated in this section. CB to VB modes of operation and vice-versa and drive performance between the two modes will be experimentally presented.

The controlled state-variables; the electromagnetic torque and the stator flux linkage responses of the drives from CB to VB mode and vice-versa are illustrated in Fig. 10 (a) and (b), respectively. It is seen from the results that the proposed drive is robust to change of the mode of operation as the transition is linear and smooth. It should be noted that the ripple on the estimated flux linkage increases when the CB

mode becomes dominant. This is as expected because of the current measurement noise. The noise is filtered at high speeds by LPFs given in Fig. 3 with a cutoff frequency of 10Hz. One can deduce from (4) that the electromagnetic torque is affected by the current measurement noise at any speed, hence the high frequency ripple on the estimated torque remains similar in both modes of operations.

Because the transition occurs between the two predefined speeds, *i.e.* w_{CB}=450 r/min and w_{VB}=550 r/min, performance tests have been carried out when γ_1 in Fig. 7 is equal to γ_2. Drive robustness to change of the torque when the estimated flux is equally far from CB and VB modes of operations has been validated in Fig. 11 (a-b-c). The phase currents when the torque is 50 Nm is illustrated in Fig. 11 (d). It is seen that the current waveforms are not deteriorated during flux transition. It is worth mentioning that a rate limiter is imposed on the step torque demand to avoid uncomfortable jerk of the traction system.

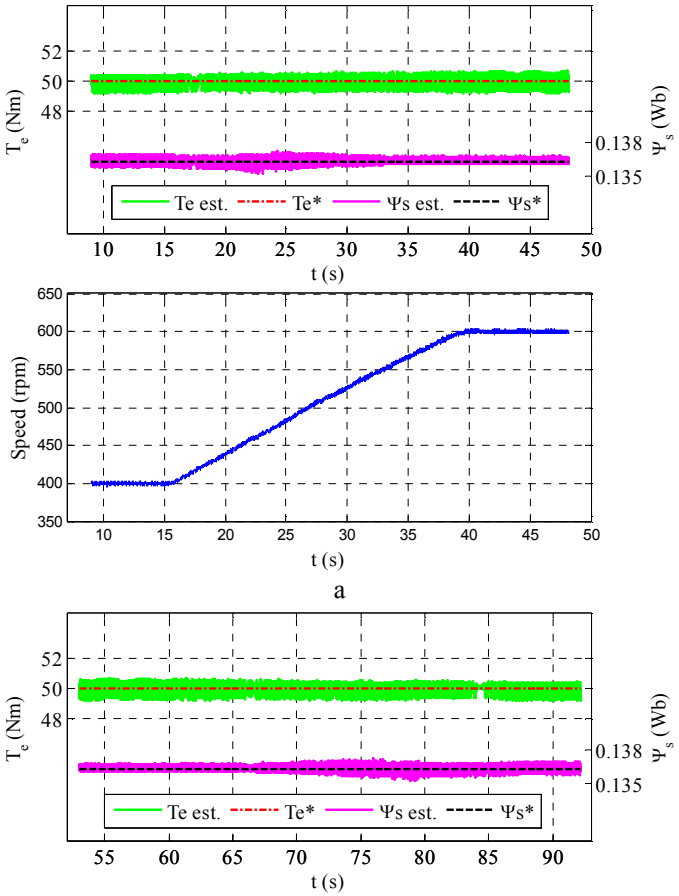

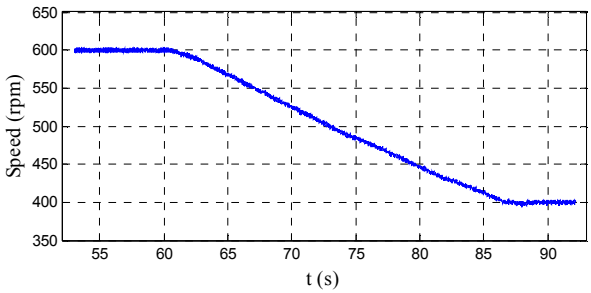

b

Fig. 10 *Drive performance from CB to VB mode and vice-versa*
a Regulated torque and flux linkage responses from $\gamma_2 = 0$ to $\gamma_1 = 0$
b Regulated torque and flux linkage responses from $\gamma_1 = 0$ to $\gamma_2 = 0$

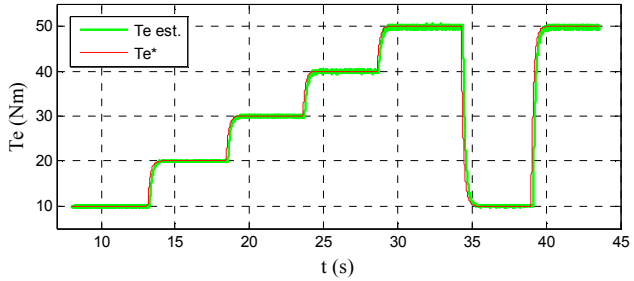

a

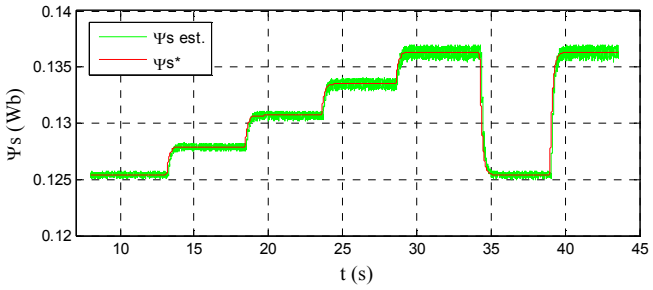

b

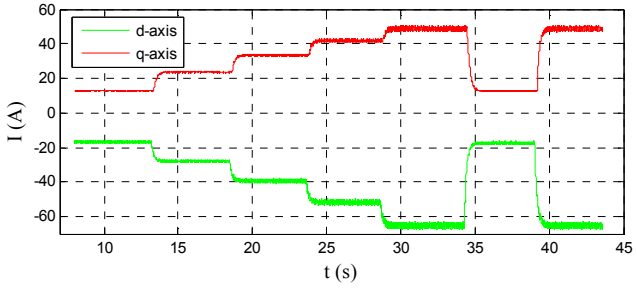

c

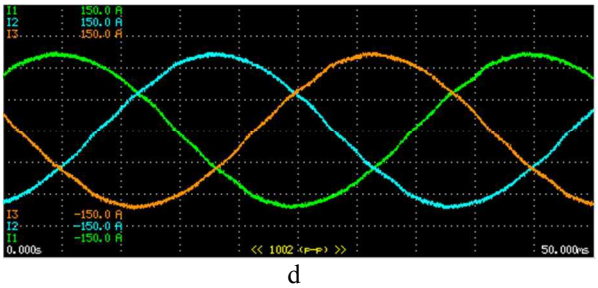

d

Fig. 11 *Drive performance at* $\gamma_1 = \gamma_2$
a Regulated electromagnetic torque responses
b Regulated stator flux linkage responses
c Measured *dq*-axis currents
d Current waveform at 50Nm torque

4.4 Field Weakening Operation

The voltage based estimations have already been validated and widely employed at high speeds in the literature [7, 8, 28].

Precise control of the transition from constant torque to field weakening region or vice versa is a challenge of IPM drives with field oriented control in the rotor reference system. In contrast, the field weakening operation in DTC drives is triggered automatically based on (9) independently from machine parameters except for the armature resistance whose variation has relatively small effect comparing to other parameter variations. Hence, FW operation can be better controlled in DTC drives.

Transient performance in FW region and the smooth transitions from MTPA to FW regions and vice-versa are illustrated in Fig. 12 when the drive operates in VB mode at 20 Nm torque. The FW is automatically triggered at the speed of 1709 r/min by (9). It is seen that the estimated flux in the constant torque region has lower ripple than that in the FW region as the current measurement noise appears when (9) is imposed to weaken the flux (magnetic field).

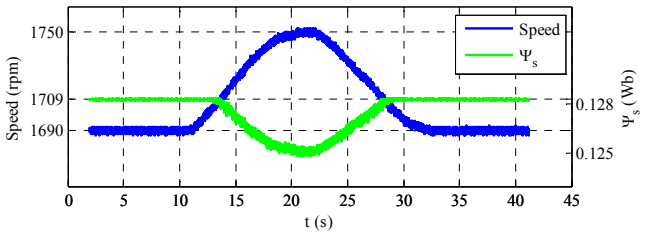

Fig. 12 *Smooth FW to MTPA and MTPA to FW transition validation*

5.Conclusion

Performance deteriorations associated with a large number of state-of-the-art DTC drives due to the cross interference and nonlinear flux transition trajectory has been addressed in this paper. It has been validated that the extremely poor VB estimation significantly deteriorates the drive performance at low speeds despite the CB mode is expected to be dominant. In addition, it has been shown that the drives with conventional Gopinath style closed loop observers suffer from poor performance during flux transitions. To

address these problems, an alternative combination of the current and voltage based estimations have been proposed with a linear flux transition trajectory. The proposed scheme is simple to implement, and results in significant improvement on the drive performance. Superiority and effectiveness of the proposed combination have been validated by experimental results of a 10 kW IPM drive which is designed for electric vehicle applications.

6.References

[1] H. Yihua, G. Chun, H. Sideng, C. Wenping, W. Xiaoming, and S. Finney, "Winding-centre-tapped switched reluctance motor drive for multi-source charging in electric vehicle applications," *Power Electronics, IET,* vol. 8, pp. 2067-2075, 2015.
[2] C. K. Lin, T. H. Liu, and S. H. Yang, "Nonlinear position controller design with input-output linearisation technique for an interior permanent magnet synchronous motor control system," *Power Electronics, IET,* vol. 1, pp. 14-26, 2008.
[3] W. Shaowei and S. Wan, "Full digital deadbeat speed control for permanent magnet synchronous motor with load compensation," *Power Electronics, IET,* vol. 6, pp. 634-641, 2013.
[4] Y. Sozer, D. A. Torrey, and E. Mese, "Adaptive predictive current control technique for permanent magnet synchronous motors," *Power Electronics, IET,* vol. 6, pp. 9-19, 2013.
[5] T. Sun, J. Wang, M. Koc, and X. Chen, "Self-Learning MTPA Control of Interior Permanent Magnet Synchronous Machine Drives Based on Virtual Signal Injection," *IEEE Transactions on Industry Applications,* vol. PP, pp. 1-1, 2016.
[6] H. Saberi, M. Sabahi, M. B. B. Sharifian, and M. Feyzi, "Improved sensorless direct torque control method using adaptive flux observer," *Power Electronics, IET,* vol. 7, pp. 1675-1684, 2014.
[7] Y. Inoue, S. Morimoto, and M. Sanada, "Control Method Suitable for Direct-Torque-Control-Based Motor Drive System Satisfying Voltage and Current Limitations," *Industry Applications, IEEE Transactions on,* vol. 48, pp. 970-976, 2012.
[8] Y. Inoue, S. Morimoto, and M. Sanada, "Comparative Study of PMSM Drive Systems Based on Current Control and Direct Torque Control in Flux-Weakening Control Region," *Industry Applications, IEEE Transactions on,* vol. 48, pp. 2382-2389, 2012.
[9] P. L. Jansen and R. D. Lorenz, "A physically insightful approach to the design and accuracy assessment of flux observers for field oriented induction machine drives," *Industry Applications, IEEE Transactions on,* vol. 30, pp. 101-110, 1994.
[10] T. Sun, J. Wang, and M. Koc, "Virtual Signal Injection Based Direct Flux Vector Control of IPMSM Drives," *IEEE Transactions on Industrial Electronics,* vol. PP, pp. 1-1, 2016.
[11] X. Wei and R. D. Lorenz, "Reduced Parameter Sensitivity Stator Flux Linkage Observer in Deadbeat-Direct Torque and Flux Control for IPMSMs," *Industry Applications, IEEE Transactions on,* vol. 50, pp. 2626-2636, 2014.
[12] C. Chan-Hee, S. Jul-Ki, and R. D. Lorenz, "Wide-Speed Direct Torque and Flux Control for Interior PM Synchronous Motors Operating at Voltage and Current Limits," *Industry Applications, IEEE Transactions on,* vol. 49, pp. 109-117, 2013.
[13] G. Pellegrino, E. Armando, and P. Guglielmi, "Direct-Flux Vector Control of IPM Motor Drives in the Maximum Torque Per Voltage Speed Range," *Industrial Electronics, IEEE Transactions on,* vol. 59, pp. 3780-3788, 2012.
[14] G. Pellegrino, E. Armando, and P. Guglielmi, "Direct Flux Field-Oriented Control of IPM Drives With Variable DC Link in the Field-Weakening Region," *Industry Applications, IEEE Transactions on,* vol. 45, pp. 1619-1627, 2009.
[15] Y. Anno and S. Seung-Ki, "Design of Flux Observer Robust to Interior Permanent-Magnet Synchronous Motor Flux Variation," *Industry Applications, IEEE Transactions on,* vol. 45, pp. 1670-1677, 2009.
[16] G. Pellegrino, R. I. Bojoi, and P. Guglielmi, "Unified Direct-Flux Vector Control for AC Motor Drives," *Industry Applications, IEEE Transactions on,* vol. 47, pp. 2093-2102, 2011.
[17] G. Pellegrino, B. Boazzo, and T. Jahns, "Plug-in, Direct Flux Vector Control of PM Synchronous Machine Drives," *Industry Applications, IEEE Transactions on,* vol. PP, pp. 1-1, 2015.
[18] B. Boazzo and G. Pellegrino, "Model Based, Direct Flux Vector Control of Permanent Magnet Synchronous Motor Drives," *Industry Applications, IEEE Transactions on,* vol. PP, pp. 1-1, 2015.
[19] X. Wei and R. D. Lorenz, "High frequency injection-based stator flux linkage and torque estimation for DB-DTFC implementation on IPMSMs considering cross-saturation effects," in *Energy Conversion Congress and Exposition (ECCE), 2013 IEEE*, 2013, pp. 844-851.
[20] W. Yukai, S. Tobayashi, and R. D. Lorenz, "Deadbeat-direct torque and flux control on low switching frequency induction machine drives using the enhanced flux observer and torque model," in *Energy Conversion Congress and Exposition (ECCE), 2013 IEEE*, 2013, pp. 1786-1793.
[21] L. Jae Suk, C. Chan-Hee, S. Jul-Ki, and R. D. Lorenz, "Deadbeat-Direct Torque and Flux Control of Interior Permanent Magnet Synchronous Machines With Discrete Time Stator Current and Stator Flux Linkage Observer," *Industry Applications, IEEE Transactions on,* vol. 47, pp. 1749-1758, 2011.
[22] Y. Anno, S. Seung-Ki, L. Dong-Cheol, and J. Cha-Seung, "Novel Speed and Rotor Position Estimation Strategy Using a Dual Observer for Low-Resolution Position Sensors," *Power Electronics, IEEE Transactions on,* vol. 24, pp. 2897-2906, 2009.
[23] K. Jang-Hwan, C. Jong-Woo, and S. Seung-Ki, "Novel rotor-flux observer using observer characteristic function in complex vector space for field-oriented induction motor drives," *Industry Applications, IEEE Transactions on,* vol. 38, pp. 1334-1343, 2002.
[24] M. Koc, J. Wang, and T. Sun, "An Inverter Nonlinearity Independent Flux Observer for Direct Torque Controlled High Performance Interior Permanent Magnet Brushless AC Drives," *Power Electronics, IEEE Transactions on,* vol. PP, pp. 1-1, 2016.
[25] B. Singh, S. Jain, and S. Dwivedi, "Torque ripple reduction technique with improved flux response for a direct torque control induction motor drive," *Power Electronics, IET,* vol. 6, pp. 326-342, 2013.
[26] X. Chen, J. Wang, B. Sen, P. Lazari, and T. Sun, "A High-Fidelity and Computationally Efficient Model for Interior Permanent-Magnet Machines Considering the Magnetic Saturation, Spatial Harmonics, and Iron Loss Effect," *IEEE Transactions on Industrial Electronics,* vol. 62, pp. 4044-4055, 2015.
[27] T. Sun, J. Wang, and X. Chen, "Maximum Torque per Ampere (MTPA) Control for Interior Permanent Magnet Synchronous Machine Drives Based on Virtual Signal Injection," *Power Electronics, IEEE Transactions on,* vol. PP, pp. 1-1, 2014.

[28] M. E. Haque and M. F. Rahman, "Incorporating control trajectories with the direct torque control scheme of interior permanent magnet synchronous motor drive," *Electric Power Applications, IET,* vol. 3, pp. 93-101, 2009.